Inorganic nanocarriers based on calcium carbonate and silica oxide for passive breast cancer targeting

Alisa S. Postovalova [ab] * [iD], Yulia A. Tishchenko [bc], Vladislava A. Rusakova [c],
Timofey E. Karpov [b], Nina V. Gavrilova [de], Anna Rogova [b] [iD],
Irina A. Gorbunova [a] [iD], Alexander S. Timin [b] [iD]

a: ITMO University, Saint-Petersburg 194021, Russia
b: Laboratory of nano- and microencapsulation of biologically active substances, Peter the Great St. Petersburg Polytechnic University, Saint-Petersburg 194021, Russia
c: St. Petersburg Academic University, Saint-Petersburg 194021, Russia
d: Laboratory of intracellular signaling and transport, Smorodintsev Research Institute of Influenza, Ministry of Health of the Russian Federation, Saint-Petersburg 197376, Russia
e: Research complex "Immunobiotechnology and gene therapy", Peter the Great St. Petersburg Polytechnic University, Saint-Petersburg 194021, Russia
* Corresponding author: alisa_postovalova@mail.ru

This paper belongs to a Regular Issue.

Abstract

Nanoparticles (NPs) are widely used platforms for delivery of various biologically active compounds. Unfortunately, there is a lack of comprehensive investigations that would include a few types of NPs with different physicochemical parameters and their potential use as delivery systems in one tumor model. Therefore, to achieve therapeutic effect via nanocarrier with therapeutic agent, the properties of the developed NPs must be clearly defined. Herein, we report the development and modification of ^{99m}Tc and Cy5-labeled NPs based on calcium carbonate (CaCO$_3$) and silica oxide (SiO$_2$) to investigate in vitro and in vivo distribution on an example of a breast cancer model. We describe the synthesis and characterization of these NPs, including their morphology, size distribution, stability in biological media and cytotoxicity. Transmission electron microscopy (TEM), confocal laser scanning microscopy (CLSM), dynamic light scattering (DLS), Fourier transform infrared spectroscopy (FTIR), direct radiometry analysis, and histology were used to collect all data. The cellular uptake of NPs on 4T1 cell line was shown *in vitro* and *in vivo*. As a result, we demonstrated that these NPs are non-toxic, biocompatible, and stable system to use for delivery of bioactive compounds into breast cancer.

Key findings

● CaCO$_3$ and SiO$_2$ NPs can be a platform for delivery to breast cancer.

● Controlling the size and structure of CaCO$_3$ and SiO$_2$ NPs allows maintaining their efficient accumulation in a tumor.

● CaCO$_3$ and SiO$_2$ NPs accumulated in the breast cancer tumor with 1.62% ± 0.3% and 2.48% ± 0.4% ID/g, respectively.

1. Introduction

Application of various types of inorganic nanoparticles (NPs) is of particular interest for delivery of biologically active, against malignant tumors, compounds [1–3]. Food and Drug Administration (FDA) approved biomaterials are required for the synthesis of NPs. Due to their advantages, like stability, controllable surface modification and drug release, NPs are ideal candidates for the clinical applications. Among plenty of investigated biocompatible materials used for synthesis of NPs, calcium carbonate (CaCO$_3$) and silica oxide (SiO$_2$) draw the most attention. Ca^{2+} is the element that is present in human body. Due to the

biocompatibility, high loading capacity and porosity suitable for therapeutic molecule accommodation, $CaCO_3$ repossesses remarkable advantages in drug delivery systems [4]. Moreover, it was noted that $CaCO_3$ NPs can be effectively loaded with various bioactive components to treat malignant tumors [5, 6]. $CaCO_3$ NPs can be obtained with a chemical co-precipitation method. The main issue of co-precipitation method used for synthesis of $CaCO_3$ NPs is controlling the size distribution [7]. $CaCO_3$ NPs obtained with this technique are non-toxic and biocompatible [8]. Meanwhile, SiO_2 is a widely used biomaterial in nanomedicine. Due to high excellent adsorption capacity and chemical stability, SiO_2 is widely used for the synthesis of NPs [9, 10]. Sol-gel method [11] is one of the best methods for the preparation of SiO_2 NPs. In particular, this technique is extensively used because of easy methodology, soft conditions, and possibility for controlling the size of obtained NPs [12]. In fact, for biodistribution investigation and accumulation efficacy in tumor site, NPs parameters such as size and charge should be comparable. Thus, the NPs with similar parameters could be obtained via modified Stöber sol-gel method. In addition, different organic additives can be used for surface modification of NPs with precise shapes and structures. In this work, we adjusted the synthetic parameters (salt concentrations, process temperature, stirring time and velocity) to develop SiO_2 NPs using sol-gel method and $CaCO_3$ NPs using co-precipitation technic in the presence of polyacrylic acid (PAA) as an organic additive to improve colloidal stability of these NPs [13].

The surface modification of described NPs allows to perform conjugation with diagnostic isotope and fluorescent dyes for *in vitro* and *in vivo* NPs visualization [14,15]. According to the previous studies, we can highlight appropriate variants of diagnostic agents for modification of NPs, which include 99m-technetium (^{99m}Tc) and Cyanine 5 [16]. Thus, these diagnostic agents were used for visualization to detect the biodistribution of developed NPs. Despite of the great potential of described NPs, there is a lack of information about their biodistribution and tumor accumulation of functionalized NPs with one particular cancer model. In fact, it prevents introducing $CaCO_3$ and SiO_2 NPs as nanocarriers for delivery of therapeutic molecules to treat malignant tumor.

The limitations of conventional therapy induce the treatment paradigm shift toward the use of tumor-specific targeting, which may improve therapeutic efficacy. New combined therapies with the use of NPs are more promising than monotherapies. For instance, combined chemo-radiotherapy with the use of SiO_2 NPs leads to two times higher efficiency compared to conventional therapy [17]. Nevertheless, there is still quite a lack of information in this field.

Due to the effect of enhanced permeability and retention (EPR) through specific passive targeting, the side effects associated with the chemotherapeutic agent are ultimately reduced, and the antitumor effect is enhanced. Passive, nonspecific targeting is driven by NPs, reduced sizes and unique properties, such as surface modifications, surface charge or nonspecific adhesion, which can lead to reaching organs with porous endothelial capillaries (liver, spleen), facilitating the crossing of specialized epithelium by NPs and penetration into the cell cytoplasm [18]. For example, in the case of cancer, the phenomenon of EPR is observed due to the specific tumor microenvironment, intense angiogenesis, uncontrollable growth of capillary net, etc.

The physicochemical properties of NPs have a significant impact on their biocompatibility and biodistribution. In order to address the biosafety of NPs, it is necessary to perform full characterization [19]. The characteristic feature of NPs, such as size, shape, size distribution, surface area, shape, solubility, aggregation, etc., need to be evaluated before assessing toxicity or biocompatibility. To do this many analytical techniques have been used, including Fourier transform infrared spectroscopy (FTIR), dynamic light scattering (DLS), scanning electron microscopy (SEM), transmission electron microscopy (TEM), atomic force microscopy (AFM), and so on [20]. Thus, it is very important to compare physicochemical properties of $CaCO_3$ and SiO_2 NPs. There is a lack of comparative knowledge of delivery efficacy of $CaCO_3$ and SiO_2 NPs towards breast cancer.

2. Materials and methods

2.1. Materials

Calcium chloride dihydrate ($CaCl_2·2H_2O$, $M_W = 147.01$), anhydrous sodium carbonate (Na_2CO_3, $M_W = 105.99$) and polyacrylic acid (PAA, No. 32667) were obtained from Sigma-Aldrich (Germany). Tetraethylorthosilicate (TEOS, 99%) and ethanol (EtOH, 99.9%) were purchased from Merck (Germany). Purified water with a specific resistivity higher than 18.2 MΩ cm^{-1} from a three-stage Milli-Q Plus 185 purification system was used. Cyanine5 (Cy5) dye, obtained from Lumiprobe Life Science solutions (Cockeysville, MD, USA), Alexa Fluor 488 (Thermo Fisher Scientific) and Propidium Iodide (PI) (Molecular Probes, Eugene, OR) were used for CLSM cellular visualization. Bovine serum albumin (BSA, 66 kDa) was bought in CSL Behring (Switzerland), dimethyl sulfoxide (DMSO) was purchased from Sigma chemical company. For ^{99m}Tc radiolabeling of NPs Tin(II) chloride dihydrate ($SnCl_2·2H_2O$, 98%) was purchased from Merck (Germany), hydrochloric acid (>35%, TraceSELECT) was purchased from Honeywell-Fluka (USA). Sodium hydroxide (BioXtra, ≥98%) and TWEEN® 80 were purchased from Sigma-Aldrich (Germany). The 4T1 cells were maintained in RPMI 1640 medium containing 10% of fetal bovine serum (FBS) (HyClone, USA).

2.2. Preparation of NPs

2.2.1. CaCO₃ NPs

A co-precipitation reaction was used to obtain polymer functionalized $CaCO_3$ NPs [8, 21]. For that, 1 mL of $CaCl_2$ aqueous solution (0.1 M) was added to 1 mL of PAA aqueous

solution (3.0 mg/mL) and stirred at room temperature for 1 h. Then, 1 mL of Na_2CO_3 aqueous solution (0.1 M) was added to the suspension. The final mixture was gently stirred for 1 h under the same conditions. Then, the suspension was washed multiple times with ethanol and purified by centrifugation for 3 min at 13.000 rpm after the reaction. Finally, the pellets were obtained and stored for further investigations.

2.2.2. SiO₂ NPs

The synthesis of SiO_2 NPs was performed using the modified sol-gel method [22]. First, 8.75 mL of 99% ethanol was mixed with 2.40 mL of Milli-Q water. After 5 min, 65 µL of 99% tetraethylorthosilicate (TEOS) and 390 µL of ammonia aqueous solution ($NH_3 \cdot H_2O$, 37%) were added to the solution drop by drop. The final mixture was vigorously stirred for 2 h. Next, the entire contents were poured into 2 mL tubes (Eppendorf, Germany) and centrifuged for 5 min at 12000 rpm. The formed SiO_2 NPs were washed by centrifugation at 12000 rpm for 5 min. The washing step was repeated four times: once with 99% ethanol and three times with Milli-Q water.

2.3. Radio- and fluorescent NPs functionalization reparations

2.3.1. Radiolabelling with ⁹⁹ᵐTc

The $CaCO_3$ and SiO_2 NPs were obtained as described above. Then, 300 µL of $SnCl_2$ (7 mg/mL, 2% HCl solution) and 1 µL of Tween 80 were added to each pellet with NPs (200 µg). The suspension was carefully resuspended, and 100 µL of $^{99m}TcO_4^-$ (solution in 0.9% NaCl) was added to the suspension of NPs. The final suspension of NPs was diluted up to 1 mL using 0.9% NaCl solution. The samples were incubated in a thermomixer for 1 h (1000 rpm, 25 °C). Then, the pH of the reaction was adjusted to pH 6.5–7.0 with 1 M NaOH. The radiolabeled NPs were washed 3 times (12.000 rpm, 5 min) and resuspended in 1 mL of 0.9% NaCl solution. The radiolabeling procedure was presented in previous work [16].

2.3.2. Fluorescent labelling with Cy5 de

2.3.2.1. Formation of Cy5-BSA complex

BSA was fluorescently labeled with Cy5 using the method described previously [23]. For that, 144 mg of BSA was added to 40 mL of PBS (pH 7.4) to a final concentration of 3.85 mg/mL. Further, 10 µg of Cy5 was resuspended in 4.4 mL of DMSO. Next, the dye mixture was combined with BSA and incubated for 24 h at 4 °C. Then, the unbound dye was removed via dialysis procedure [24]. For this, the resulting solution was poured into a dialysis bag, which was then placed in a beaker and stirred for 3 d (500 rpm, 4 °C). The water with non-reacted dye was changed every 24 h.

2.3.2.2 Cy5-labeling of CaCO₃ NPs

To obtain Cy5-labeled $CaCO_3$ NPs, 1 mL of 0.1. M $CaCl_2$ aqueous solution was added separately to 500 µL of the Cy5-BSA

complex and then stirred at room temperature for 1 h. After that, 1 mL of PAA aqueous solution (3.0 mg/mL) was added, and stirring was continued for 1 h. Next, 1 mL of Na_2CO_3 aqueous solution (0.1 M) was added to the resulting mixture and left for 1 h. The resulting solution was washed multiple times with ethanol and purified by centrifugation for 3 min at 13000 rpm after the reaction until there was no free dye left. Finally, the solvent was exchanged to PBS for further use.

2.3.2.3 Cy5-labeling of SiO₂ NPs

To obtain Cy5-labeled SiO_2 NPs, 500 µL of Cy5-BSA (5 mg/mL) was added to NPs during the sol-gel synthesis using the co-precipitation method. Finally, the SiO_2 NPs with Cy5 were washed twice (12 000 rpm, 3 min) with Milli-Q water to remove the unbound dye.

2.4. Characterization of NPs

2.4.1. Transmission electron microscopy

The shape and size of the obtained NPs were analyzed using transmission electron microscope (TEM) with a JEOL JEM-1400 model (JEOL LTD, Tokyo, Japan) operated at the voltage of 100 kV.

2.4.2. DLS and zeta potential

The hydrodynamic diameter (D_h) of the NPs was measured using BK Winner803 DLS Nano Particle Size Analyzer. The zeta potential of the $CaCO_3$ and SiO_2 NPs was determined in phosphate buffered solution (PBS) with pH 7.4 using ZetaSizer Ultra device (Malvern Instruments, UK). Three measurements were made for each sample.

2.4.3. FTIR

Fourier transform infrared spectroscopy (Tensor 27, Bruker, Germany) was used to characterize the functional groups of $CaCO_3$ and SiO_2 NPs. For each spectrum, 50 scans between the wavenumbers of 4000 and 400 cm⁻¹ were recorded in an attenuated total reflection mode.

2.4.4. Cellular uptake studies

To visualize cellular uptake of the NPs, the 4T1 cells were seeded into 24-well plate ($1.0 \cdot 10^4$ per well). After incubation, the Cy5-fluorescent labeled NPs were added to the cells at different concentrations (0.5 mg/mL, 1.0 mg/mL, and 2.0 mg/mL), and the cells were left overnight. Next day, the cell cytoskeletons were stained with phalloidin conjugated with AlexaFluor 488 (AF488), and the cell nuclei were stained blue with Propidium Iodide (PI). Cellular uptake of the NPs was visualized using a confocal laser scanning microscope (CLSM), Leica TCS SP8 (Germany). To visualize the cell cytoskeletons and cell nuclei, an argon laser emitting at 488 nm and a helium-neon laser emitting at 543 nm were used, respectively. To visualize Cy5-labeled NPs, a helium-neon laser emitting at 633 nm was used. The confocal pinhole was set to 1 Airy unit, and the images were taken with an HC PL FLUOTAR 10x/0.30 PH2 Objective.

2.4.5. Tumor model formation

For *in vivo* studies, healthy, immunocompetent Balb/c mice (males, eight weeks old, 18–22 g) from the St. Petersburg center of laboratory animals "Rappolovo" of the national research center "Kurchatov Institute" and were used. The mice were housed in cages under controlled environmental conditions, with access to food and water provided *ad libitum*, and were quarantined in a specific pathogen-free environment.

To establish the 4T1 metastatic tumor model, male Balb/c mice (eight weeks old, 18–22 g) were intravenously injected with 4T1 cells (0.1 mL, 10^6 cells/mL) through the tail vein. On the 10th d after the infusion of tumor cells, the mice were randomly divided into experimental groups, and the therapy was started. All the animal experiment protocols were approved by the veterinary office of the Russian Research Center for Radiology and Surgical Technologies and its local ethics committee.

2.4.6. Radiometry/dosimetry of *ex vivo* main organs and tumours

Direct radiometry analysis of the biodistribution of the ^{99m}Tc-labeled NPs in the tumor-bearing Balb/c mice was performed using a TRIATHLER portable spectrometric radiometer (Hidex Oy, Finland). Each animal was injected intravenously with ^{99m}Tc-labeled $CaCO_3$ and SiO_2 NPs in the same dose (12 MBq, 100 µL, 2 mg/mL). The animals were sacrificed. Then, the main organs (the heart, lungs, liver, spleen, kidneys) and tumors were removed from the body and weighed. Total radioactivity for each tested sample was calculated as the percentage of the injected activity adjusted by the weight of tissues (% dose/g).

2.4.7. Fluorescent histology of tumour tissue

Histological tissue sections were obtained from euthanized mice 24 h after the injection of Cy5-labeled $CaCO_3$ and SiO_2 NPs. The biopsy samples were isolated from the tumors and cut into 2–4 µm thick sections using a HM 340E rotary microtome (Thermo Scientific). Next, the samples were placed in a solution of PI (10 mg/mL) for 5 min to fluorescently stain the cell nuclei. After that, the sections were washed in PBS solution and enclosed in a glycergel. Then, the fixed samples were visualized under CLSM (with an objective EC PlanNeofluar 40x/1.30 Oil DIC).

3. Results and Discussion

3.1. Preparation

3.1.1. Preparation of $CaCO_3$ NPs

The synthesis of polymer functionalized $CaCO_3$ NPs was carried out using a co-precipitation reaction between aqueous solutions of $CaCl_2$ and Na_2CO_3 in the presence of PAA (Figure 1A). The PAA is an anionic polymer (negatively charged) containing carboxylic groups with relative electrostatic interaction with calcium ions, which influence the morphology and crystal growth of $CaCO_3$. Additional surface modification affects the aggregation

and crystallization behavior of $CaCO_3$ NPs. TEM images showed that the NPs changed their morphology from irregular shape to spherical shape when the concentration of PAA was increased (Figure 2a). The $CaCO_3$ NPs were not universally spherical, and their surface was slightly rough. Some NPs were observed to be interconnected with each other. In fact, PAA was negatively charged and could interact with calcium ions to aggregate around it. Thus, increasing the PAA concentration influences the morphology of $CaCO_3$ NPs and promotes their spherical form.

3.1.2. Preparation of SiO_2 NPs

SiO_2 NPs were synthesized using the previously described sol-gel method [25], which involves the hydrolysis reaction of TEOS in water and ethanol in the presence of ammonium hydroxide solution with forming $Si(OH)_4$. The scheme of synthesis is presented in Figure 2b. The hydrolysis reaction of TEOS proceeds through the formation of reactive Si–OH species and subsequent condensation of bonds leading to the formation of the Si–O–Si bridges [24, 26]. The condensation of the supersaturated silicic acid was indicated by an increasing opalescence of the mixture starting 2–10 min after adding the TEOS [25].

3.2. Characterization

3.2.1. Size, morphology, TEM and DLS characterization

The optimal parameters were selected to obtain $CaCO_3$ NPs and SiO_2 NPs. TEM revealed $CaCO_3$ NPs and SiO_2 NPs with the size distribution in the range of 50–120 nm (Figure 2a). NPs were described as spherical with slightly rough surface for SiO_2 NPs and scalenohedral for $CaCO_3$ NPs. Meanwhile, the size distribution of $CaCO_3$ and SiO_2 NPs was estimated by measuring the hydrodynamic diameter (D_h) values in an aqueous solution. The average D_h values according to the DLS analysis were 70–120 and 100–150 nm for modified $CaCO_3$ and SiO_2 NPs, respectively (Figure 2b). Electrochemical surface features of modified NPs were observed through zeta potential measurements. The zeta potentials in deionized water of modified SiO_2 and $CaCO_3$ were –0.96 and –10 mV, respectively. The delivery efficacy of NPs with neutral zeta potential or one in the range of –10/+10 mV was reported to be higher than that of NPs with positive (> 10 mV) or negative (<–10 mV) zeta potential [27].
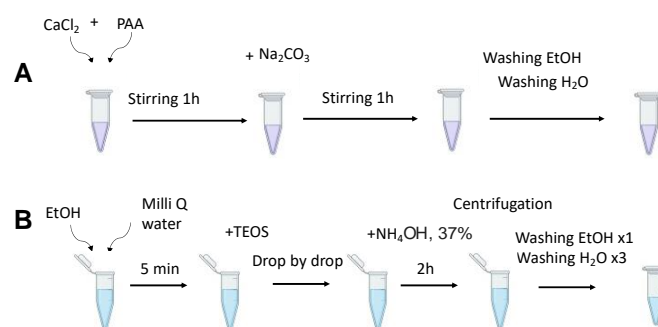

Figure 1 Scheme of $CaCO_3$ NPs synthesis (a). Scheme of SiO_2 NPs synthesis (b).

The less negatively charged $CaCO_3$ and SiO_2 NPs were chosen for biodistribution estimation *in vivo* [28–30]. Tumor accumulation was higher with zeta potential <-10 mV. Thus, appropriate zeta potentials of NPs increase their delivery efficacy.

PAA modified $CaCO_3$ NPs did not express any significant aggregation compared to NPs obtained without PAA coating (Figure 3a). At the same time, modified SiO_2 showed spherical morphology (Figure 3b). The presence of $SnCl_2$ used for radiolabeling of SiO_2 NPs did not influence on the morphology of the final products.

To further study the structural characteristics of developed NPs, FTIR spectra measurements of $CaCO_3$ and SiO_2 NPs were performed (Figure 4). According to Figure 4a, the FTIR spectrum of $CaCO_3$ NPs is characterized by the presence of stretching vibrations of the C–O approximately at 1412 cm^{-1} and bending vibrations of the C–O approximately at 862 and 683 cm^{-1} [31]. Meanwhile, the FTIR spectrum of SiO_2 NPs displays three characteristic absorption peaks approximately at 1070, 950 and 800 cm^{-1} that shows the Si–O–Si stretching vibration bonding (Figure 4b). Absence of signals in the range from 3000 to 4000 cm^{-1} indicated the absence of H_2O molecules (in this range, vibrations of O–H bonds of water molecules appear) [32].

3.2.2. Cell uptake and distribution assay

The cellular uptake study was performed to reveal the internalization and association of $CaCO_3$ and SiO_2 NPs with breast cancer cells (4T1). For this, CLSM imaging and flow cytometry analysis were used. The cell nucleus was stained with PI and the actin cytoskeleton was labeled with Alexa Flour 488 Phalloidin. Meanwhile, Cy5-labeled $CaCO_3$ and SiO_2 NPs were used. The Cy5-labeled NPs (2 mg/mL) were incubated with cells for 24 h.

CLSM displayed significant uptake and distribution of Cy5-labeled NPs within 4T1 cells (Figure 5a). The quantitative data of cell association was ~56.5% for $CaCO_3$ NPs and ~64.7% for SiO_2 NPs (Figure 5b). The cell viability was >83% for wide concentrations of NPs (Figure 5c). These observations demonstrated that two types of Cy5-labeled NPs have high cellular uptake in the 4T1 tumor.

The quantitative assessment of biodistribution of the ^{99m}Tc-labeled NPs was evaluated with direct radiometry analysis. After 24 h, the mice were euthanized, and the organs (the heart, lungs, liver, spleen, kidneys) and tumors were collected for the analysis. The obtained radioactivity data are presented in Table 1 in dose % per gram values (% dose/g).

According to Table 1, the ^{99m}Tc-labeled NPs were mainly accumulated in the liver (~82–84%) and only small amounts of NPs were detected in the tumor (<3%). The radioactivity in the 4T1 tumors was higher in ^{99m}Tc-labeled SiO_2 NPs than in ^{99m}Tc-labeled $CaCO_3$ NPs: 2.48%±0.4% and 1.62%±0.3%. The higher percentage of ^{99m}Tc-labeled

NPs accumulation was detected in the liver due to mononuclear phagocyte system, which agrees with the literature data [18]. The NPs can accumulate in the liver due to their size, shape, surface coating, and the animal model [32]. The exception is NPs smaller than 6 nm, which can be filtered by kidneys and excreted into the urine [33].

3.2.3. Histological analysis

The fluorescent histological analysis demonstrated the distribution of Cy5-labeled $CaCO_3$ and SiO_2 NPs within tumor 4T1 tissues (Figure 6). The results of fluorescent histological analysis revealed the same trend in accumulation of NPs as it was observed in case of radiometry analysis. It could be explained by tumor model heterogeneity, variety of blood vessels and network of microcapillaries, supplying tumor with nutrients and oxygen [34, 35].
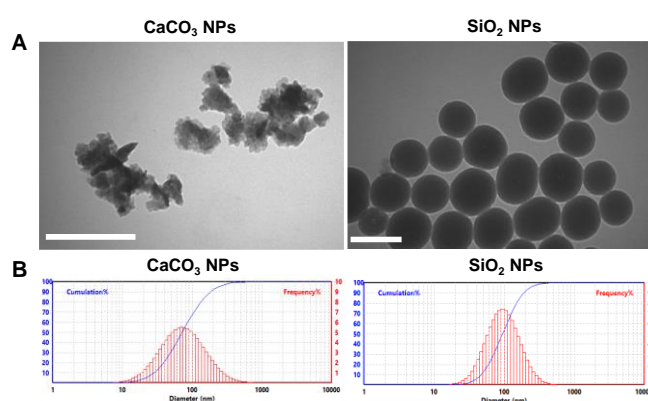

Figure 2 TEM images of $CaCO_3$ NPs (left) and SiO_2 NPs (right) (a). Scale bar = 200 nm. DLS analysis of NPs hydrodynamic diameters (D_h) (b).
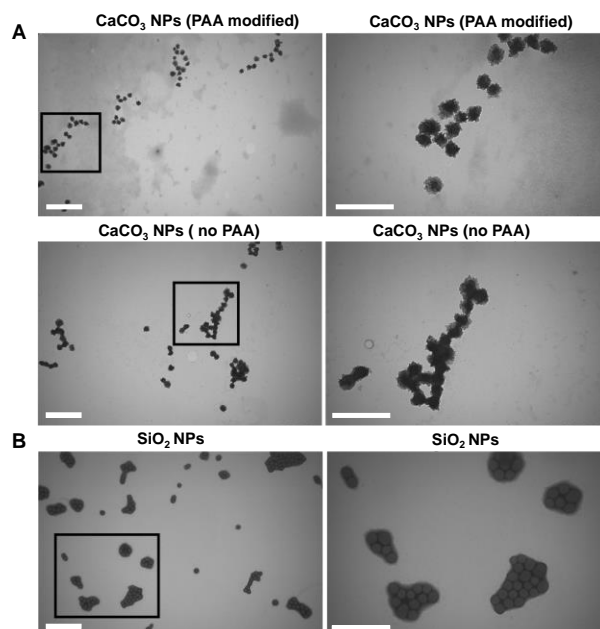

Figure 3 TEM images of $CaCO_3$ NPs (PAA/no PAA modification) (a). TEM images of SiO_2 NPs modifications with $SnCl_2$ modified for ^{99m}Tc-labeling. Scale bar = 1000 nm (left column) and 500 nm (right column) (b).

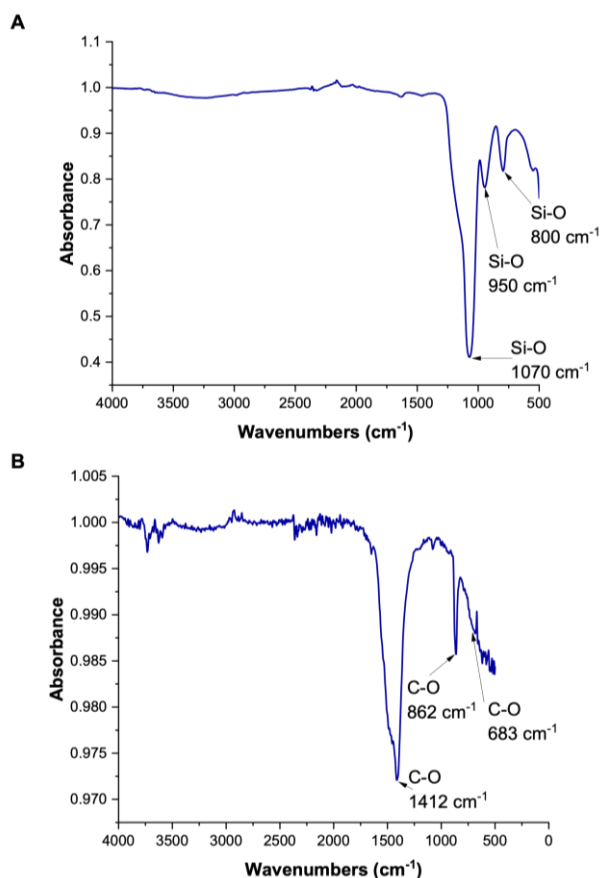**Figure 4** Fourier transform infrared (FTIR) spectra of SiO$_2$ (a) and CaCO$_3$ NPs (b).
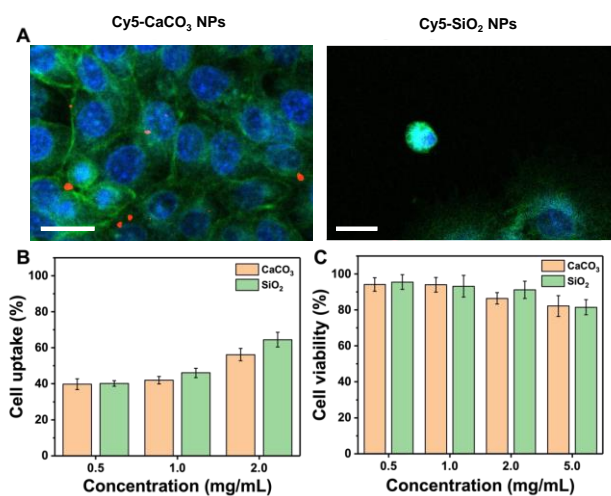

Figure 5 CLSM images of 4T1 cell line uptake incubated with CaCO$_3$ and SiO$_2$ NPs at concentration of 2 mg/mL. The cells were co-stained with AF488 (green) and PI (blue). The NPs were labeled with Cy5 (red). Scale bar = 25 μm (a). The cellular uptake efficacy of CaCO$_3$ and SiO$_2$ NPs (b). Cell toxicity of CaCO$_3$ and SiO$_2$ NPs at 0.5, 1.0, 2.0, 5.0 mg/mL concentrations to 4T1 cell line determined by flow cytometry (c).

The percentage of Cy5-labeled CaCO$_3$ NPs detected in 4T1 tumor tissue was compared with the percentage of Cy5-labeled SiO$_2$ NPs in the 4T1 tumor sample by using CLSM visualization.

4. Limitations

The main difficulties in developing carriers for drug delivery still include: 1) scaling-up synthesis of NPs for clinical practice, 2) overcoming the accumulation in biological barriers (distribution of NPs in the liver and spleen) [36] and 3) lowering carriers' toxicity. Thus, to reach scalable carrier production, the chosen strategy of using passive drug delivery of NPs without ligand-receptor selection (active targeting) gives more potential advantages for further NPs implementation in therapeutic compositions. Moreover, NPs affinity to various types of tumors is still unknown because of non-comprehensive approach to studying those aspects. However, second challenge in that case became more inevitable to stop the progress. Therefore, investigations in this field would help to find new potential non-toxic, biocompatible NPs to obtain the carrier with adaptive structure and controllable properties.

5. Conclusions

Summing up, we described the synthesis of CaCO$_3$ and SiO$_2$ NPs. These NPs were fully characterized. The synthesized NPs exhibited appropriate stability, low toxicity, and biocompatibility. ^{99m}Tc- and Cy5-labeling was performed to investigate the biodistribution of CaCO$_3$ and SiO$_2$ NPs. We can propose these NPs as potential carriers for drug delivery. In addition, the proposed synthesis methods are quite simple, cost-effective and easily scalable for further translation into clinical practice.
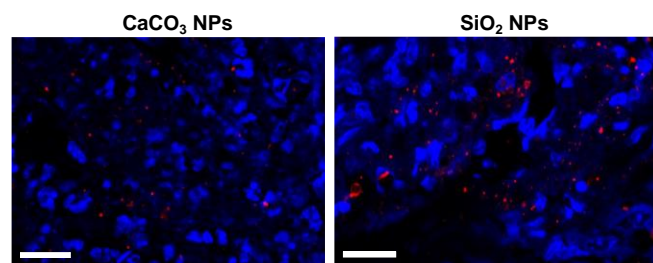

Figure 6 Comparison of Cy5-labeled CaCO$_3$ and SiO$_2$ NPs accumulation in 4T1 tumor tissue with fluorescent staining. PI colored cell nuclei and Cy5-labeled NPs visualized as red dots. Scale bars correspond to 200 μm.

Table 1 Direct radiometry analysis of main organs after injection of CaCO$_3$ and SiO$_2$ NPs.

Sample type[a]	CaCO$_3$ NPs[b]	SiO$_2$ NPs[c]
Heart	3.71±0.6%	3.95±0.3%
Lungs	2.31±0.5%	2.34±0.1%
Liver	82.2±4.2%	83.9±4.3%
Spleen	6.12±0.4%	6.0±0.3%
Kidney	2.31±0.5%	2.96±0.4%
Tumor	1.62%±0.3%	2.8%±0.4%

[a] mouse excluded organ type;

[b] radioactivity data per gram values (%dose/g);

[c] radioactivity data per gram values (%dose/g).

● **Supplementary materials**

No supplementary materials are available.

● **Funding**

● **Acknowledgments**

● **Author contributions**

Conceptualization: A.S.P., A.S.T.
Data curation: A.S.P., A.S.T.
Formal Analysis: A.S.P., A.S.T.
Funding acquisition: A.S.P., A.S.T.
Investigation: A.S.P., Y.A.T, V.A.R., A.R., T.E.K.
Methodology: A.S.P., Y.A.T, V.A.R., A.R., T.E.K.
Project administration: A.S.P., A.S.T.
Resources: A.S.P., A.S.T.
Software: A.S.P., A.S.T.
Supervision: A.S.T.
Validation: A.S.P., S.A.S., A.S.T.
Visualization: A.S.
Writing – original draft: A.S.P., S.A.S., A.S.T.
Writing – review & editing: A.S.T.

● **Conflict of interest**

The authors declare no conflict of interest.

● **Additional information**

Author IDs:

Alisa S. Postovalova, Scopus ID 57354056200;
Anna Rogova, Scopus ID 57460920100;
Timofey E. Karpov, Scopus ID 57204146848;
Alexander S. Timin, Scopus ID 55750527100.

Websites:

Peter the Great St. Petersburg Polytechnic University, https://english.spbstu.ru;
ITMO University, https://en.itmo.ru;
St. Petersburg Academic University, http://studyinspb.ru/ru/university/?id=42.

References

1. Zhou F, et al. Hyaluronan derivative decorated calcium carbonate nanoparticle as a potential platform for breast cancer synergistic therapy via blood coagulation and drug delivery. J Drug Deliv Sci Technol. 2023;83:104406. doi:10.1016/j.jddst.2023.104406

2. Huang H, et al. Smart responsive-calcium carbonate nanoparticles for dual-model cancer imaging and treatment. Ultrasonics. 2020;108:106198. doi:10.1016/j.ultras.2020.106198.

3. Barbezan AB, et al. Radioactive gold nanoparticles coated with BSA: A promising approach for prostate cancer treatment. Nanotheranostics. 2024;8(1):112–126. doi:10.7150/ntno.91507

4. Liang T, et al. Research progress of calcium carbonate nanomaterials in cancer therapy: challenge and opportunity. Front Bioeng Biotechnol. 2023;11. doi:10.3389/fbioe.2023.1266888

5. Lin C, et al. Recent Developments in CaCO$_3$ Nano-Drug Delivery Systems: Advancing Biomedicine in Tumor Diagnosis and Treatment. Pharmaceutics. 2024;16(2):275. doi:10.3390/pharmaceutics16020275

6. Li Y, et al. Calcium Carbonate/Polydopamine Composite Nanoplatform Based on TGF-β Blockade for Comfortable Cancer Immunotherapy. ACS Appl Mater Interfaces. 2024;16(3):3187–3201. doi:10.1021/acsami.3c16571

7. Maleki Dizaj S, et al. Calcium carbonate nanoparticles as cancer drug delivery system. Expert Opin Drug Deliv. 2015;12(10):1649–1660. doi:10.1517/17425247.2015.104953

8. Bahrom H, et al. Controllable Synthesis of Calcium Carbonate with Different Geometry: Comprehensive Analysis of Particle Formation, Cellular Uptake, and Biocompatibility. ACS Sustain Chem Eng. 2019;7(23):19142–19156. doi:10.1021/acssuschemeng.9b05128

9. Kim TG, et al. Synthesis of Size Controlled Spherical Silica Nanoparticles via Sol-Gel Process within Hydrophilic Solvent. J Kor Ceram Soc. 2017;54(1):49–54. doi:10.4191/kcers.2017.54.1.10

10. Wu S-H, Mou C-Y, Lin H-P. Synthesis of mesoporous silica nanoparticles. Chem Soc Rev. 2013;42(9):3862. doi:10.1039/c3cs35405a

11. Stöber W, Fink A, Bohn E. Controlled growth of monodisperse silica spheres in the micron size range. J Colloid Interface Sci. 1968;26(1):62–69. doi:10.1016/0021-9797(68)90272-5

12. Bhatt N, et al. Preparation of Silica Nano-Particles by Sol-Gel Method and Its Characterization. J Graphic Era Univer. 2021. doi:10.13052/jgeu0975-1416.927

13. Reduction diameter of CaCO$_3$ crystals by using poly acrylic acid might improve cellular uptake of encapsulated curcumin in breast cancer.

14. Zhou X, et al. Single-injection subunit vaccine for rabies prevention using lentinan as adjuvant. Int J Biol Macromol. 2024;254:128118. doi:10.1016/j.ijbiomac.2023.128118

15. Moore CJ, et al. Controlling colloidal stability of silica nanoparticles during bioconjugation reactions with proteins and improving their longer-term stability, handling and storage. J Mater Chem B. 2015;3(10):2043–2055. doi:10.1039/C4TB01915F

16. Karpov T, et al. Universal Chelator-Free Radiolabeling of Organic and Inorganic-Based Nanocarriers with Diagnostic and Therapeutic Isotopes for Internal Radiotherapy. Chem Mater. 2022;34, № 14:6593–6605. doi:10.1021/acs.chemmater.2c01507

17. Abrishami A, et al. Hybridized quantum dot, silica, and gold nanoparticles for targeted chemo-radiotherapy in colorectal cancer theranostics. Commun Biol. 2024;7(1):393. doi:10.1038/s42003-024-06043-6

18. Rabanel MJ, et al. Drug-Loaded Nanocarriers: Passive Targeting and Crossing of Biological Barriers. Curr Med Chem. 2012;19(19):3070–3102. doi:10.2174/092986712800784702

19. Shekunov BY, et al. Particle Size Analysis in Pharmaceutics: Principles, Methods and Applications. Pharm Res. 2007;24(2):203–227. doi:10.1007/s11095-006-9146-7

20. Titus D, James Jebaseelan Samuel E, Roopan SM. Nanoparticle characterization techniques. Green Synthesis, Characterization and Applications of Nanoparticles. Elsevier, 2019:303–319. doi:10.1016/B978-0-08-102579-6.00012-5

21. Muslimov AR, et al. An investigation of calcium carbonate core-shell particles for incorporation of 225Ac and sequester of daughter radionuclides: in vitro and in vivo studies. Journal of Controlled Release. 2021;330:726–737. doi:10.1016/j.jconrel.2021.01.008

22. Mahmed N, et al. Synthesis of Nanosized Silica and Silver-Doped Silica Nanoparticles for Heat Transfer Fluids Applications. Key Eng Mater. 2015;660:155–160. doi:10.4028/www.scientific.net/KEM.660.155

23. Karpov TE, et al. Impact of metallic coating on the retention of 225Ac and its daugthers within core–shell nanocarriers. J Colloid Interface Sci. 2022;608:2571–2583. doi:10.1016/j.jcis.2021.10.187

24. Timin AS, et al. Triple-responsive inorganic–organic hybrid microcapsules as a biocompatible smart platform for the delivery of small molecules. J Mater Chem B. 2016;4(45):7270–7282. doi:10.1039/C6TB02289H

25. Tabatabaei S, et al. Experimental study of the synthesis and characterisation of silica nanoparticles via the sol-gel method. J Phys Conf Ser. 2006;26:371–374. doi:10.1088/1742-6596/26/1/090

26. Nazarabady MM, Farzi G. Morphology control to design p(acrylic acid)/silica nanohybrids with controlled mechanical properties. Polymer (Guildf). 2018;143:289–297. doi:10.1016/j.polymer.2018.02.026

27. Wilhelm S, et al. Analysis of nanoparticle delivery to tumours. Nat Rev Mater. 2016;1(5):16014. doi:10.1038/natrevmats.2016.14

28. Hanafi-Bojd MY, et al. Surface functionalized mesoporous silica nanoparticles as an effective carrier for epirubicin delivery to cancer cells. Eur J Pharmac Biopharmac. 2015;89:248–258. doi:10.1016/j.ejpb.2014.12.009

29. Chang J, et al. A pH-responsive mesoporous silica nanoparticle-based drug delivery system for targeted breast cancer therapy. J Mater Chem B. 2022;10(17):3375–3385. doi:10.1039/D1TB02828F

30. Som A, et al. Calcium carbonate nanoparticles stimulate tumor metabolic reprogramming and modulate tumor metastasis. Nanomedicine. 2019;14(2):169–182. doi:10.2217/nnm-2018-0302

31. Dubey RS, Rajesh YBRD, More MA. Synthesis and Characterization of SiO_2 Nanoparticles via Sol-gel Method for Industrial Applications. Mater Today Proc. 2015;2(4–5):3575–3579. doi:10.1016/j.matpr.2015.07.098

32. Barhoum A, et al. Preparation and characterization of ultra-hydrophobic calcium carbonate nanoparticles. IOP Conf Ser Mater Sci Eng. 2014;64:012037. doi:10.1088/1757-899X/64/1/012037

33. Tsoi KM, et al. Mechanism of hard-nanomaterial clearance by the liver. Nat Mater. 2016;15(11):1212–1221. doi:10.1038/nmat4718

34. Soo Choi H, et al. Renal clearance of quantum dots. Nat Biotechnol. 2007;25(10):1165–1170. doi:10.1038/nbt1340

35. Bahcecioglu G, et al. Breast cancer models: Engineering the tumor microenvironment. Acta Biomater. 2020;106:1–21. doi:10.1016/j.actbio.2020.02.006

36. Wagenblast E, et al. A model of breast cancer heterogeneity reveals vascular mimicry as a driver of metastasis. Nat. 2015;520(7547):358–362. doi:10.1038/nature14403

37. Ejigah V, et al. Approaches to Improve Macromolecule and Nanoparticle Accumulation in the Tumor Microenvironment by the Enhanced Permeability and Retention Effect. Polymers (Basel). 2022;14(13):2601. doi:10.3390/polym14132601